Chapter 4

High Responsivity ZnO Nanorods/ PTB7 Polymer Heterojunction Based UV - Visible Photodetector

Content of this Chapter

4.1 Introduction…… 69

4.2 Experimental Methodology …….. 70

4.2.1. Materials Used and Synthesis…….. 70

4.2.2. Device Fabrication……. 72

4.3 Results and Discussion……... 72

4.3.1 Material Characterization……72

4.3.2 Electrical and Optical Characterization…….76

4.4 Conclusions…….84

Part of this work has been published as:

- **D. C. Upadhyay** et al., "High Responsivity ZnO Nanorods/ PTB7 Polymer Heterojunction Based UV - Visible Photodetector," in ***IEEE Photonics Technology Letters***, doi: 10.1109/LPT.2021.3112685. (IF: **2.451**)

Chapter 4

High Responsivity ZnO Nanorods/ PTB7 Polymer Heterojunction Based UV - Visible Photodetector

4.1 Introduction

We have already explored PCDTBT: PCBM: PbS QDs [112] and PCDTBT: PCBM: CdSe NCs [116] based organic-inorganic ternary nanocomposites based high performance wideband photodetectors in Chapter 2 and 3 respectively. However, the inorganic-organic materials-based type-2 heterostructures have been widely explored for high performance UV-Visible (UV-Vis) photodetectors in recent times [117]. In general, various nanostructures such as nanorods [118], nanoparticles [119] and quantum dots [120] of ZnO have been widely explored for the UV sensing applications due to some important properties of the ZnO such as its wide bandgap energy (~3.4 eV), high mobility, low fabrication cost, easy availability, and environment-friendly nature [119]. Heterojunctions of n-type ZnO nanostructures and p - type conjugated polymers such as P3HT [118] pentacene [121] and PEDOT: PSS [122] have also been reported by several research groups for high performance UV or UV-Vis wideband photo detectors. Srivastava et al. [121] have reported a ZnO thin film/Pentacene heterojunction-based high-performance UV-visible wideband photodetector. However, the major drawback of the pentacene is associated with the difficulty in its synthesis using low-cost solution process.

Recently, a newly synthesized low bandgap polymer namely PTB7 (poly[[4,8-bis [(2 ethylhexyl) oxy] benzo [1,2-b:4,5-b']dithiophene-2,6-diyl][3-fluoro-2-[(2ethylhexyl)carbonyl] thieno [3,4-b] thiophenediyl]] has drawn considerable attention for bulk heterojunction solar cell applications with superior performance[123]. Lim et al.[124]

have investigated higher hole transport properties of PTB7 over other polymers like the P3HT and Spiro-OMeTAD for high performance solar cells. Further, the PTB7 material has also a reasonably high hole mobility [125]. Moreover, the fabrication of solution processed high quality PTB7 thin films is much easier than that of the pentacene films[121]. Since it is relatively a new conducting polymer, it is believed that there are ample opportunities to explore this newly introduced PTB7 material photodetection applications.

In view of the above discussion, an attempt has been made to investigate the performance characteristics of an FTO/ZnO NRs/p-PTB7/MoOx/Ag structure-based UV-Vis wideband photodetector. The basic objective is to replace the ternary organic-inorganic nanocomposites reported in the previous chapter by a single high-quality polymer PTB7 for UV-Visible broadband photodetectors. Thus, both the fabrication complexity and cost of the proposed device are less than the UV-Visible detector considered in Chapter 3. The ZnO NRs material serves as ETL-cum- UV light absorption layer while the PTB7 dominantly absorbs light in the visible region. The MoOx layer serves as the HTL in the device.

4.2 Experimental Methodology

4.2.1. Materials Used and Synthesis

All the chemical reagents procured from Sigma-Aldrich, Merck chemical and ossila were used directly without any further cleansing. FTO substrates cleansing were ultrasonically done by soap solution, deionized water (DI water) and acetone for 5 min each. The ZnO QDs were synthesized by following our method reported in [126]. In this method, for the preparation of ZnO QDs, 2-methoxy ethanol and zinc acetate dihydtrate (0.5M) was mixed in a three-neck flask. The prepared solution was continuously stirred and its temperature was

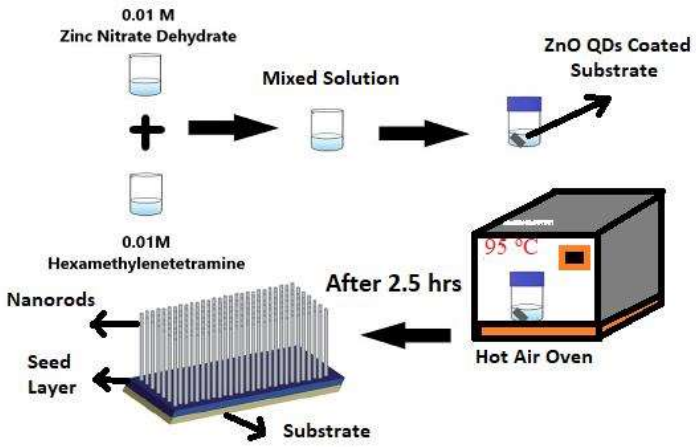

Fig.4.1: Schematic of ZnO nanorods synthesis by using low cost hydrothermal.

gradually increased to 60^0C. A this temperature, MEA (monoethanolamine) solution was injected speedily into the prepared solution and this solution after injection is again kept under continuous stirring for 24 h under nitrogen environment to obtain colloidal ZnO QDs. The ZnO QDs seed layer of thickness ~ 50 nm was then spin cast on the FTO substrate by using spin coating method at 2000 rpm for 60s and the coated seed layer was by annealed for 30 minutes at 150^0C. Finally, the ZnO nanorods were grown by hydrothermal process as described in [112], [116] with a slight modification. In this approach the ZnO QDs seed layer coated FTO substrates was kept in the laboratory glass culture vials containing hexamethylenetetramine (0.01M) and zinc nitrate dehydrate (0.01M) solution at 95 ^{o}C for 2.5 hours. Finally, after 2.5 hours the substrates with grown nanorods were taken out from the glass culture vials and washed rigorously with water (DI).At last the grown ZnO NRs samples were annealed for 40 min at 400^0C to improve adhesion and remove residual content if any [127].The complete schematic of hydrothermal synthesis of ZnO nanorods is elucidated pictorially in the Fig.4.1.

4.2.2. Device Fabrication

The procured PTB7 polymer materials from the ossila were first dissolved in chloroform (15mg/ml) followed by stirring for 15 hours in an open environment condition. The solution was then spin coated on the as-grown ZnO NRs samples at 1500 rpm for 60s to achieve the desired n-ZnO NRs/PTB7 heterojunction. The polymer concentration was deliberately kept low to allow its smooth infiltration into the ZnO nanorods [128] for achieving large interfacial area[129]. Spin coated PTB7 layer was annealed at 110 ^{0}C for 10 min. Thermal evaporation technique is used to deposit thin MoOx layer of ~ 10 nm thick on the PTB7 polymer layer. At last, silver (Ag) electrode contacts of thickness ~120 nm was also deposited by using the same thermal evaporation techniques. The calculated active area of the device was found to be 0.0314 cm^2 [111], [130]. The device was then processed for electrical and optical measurements.

4.3 Results and Discussion

4.3.1 Material Characterization

The HRSEM image for investigating the surface morphology of the ZnO NRs layer is shown in Fig.4.2 at 400 nm scale and magnified version is also shown at the top right- side corner. The grown ZnO NRs are observed to be densely packed with hexagonal cross section which very well oriented over the entire substrate. This confirms that the synthesized ZnO NRs can efficiently dissociate the exciton at the ZnO NRs/PTB7 interface to result in superior photoresponse behavior of the device [129]. The cross-sectional FE- SEM images of ZnO NRs/PTB7 bilayer and ZnO NRs layer only are shown in Fig.4.3 (a), (b), respectively.

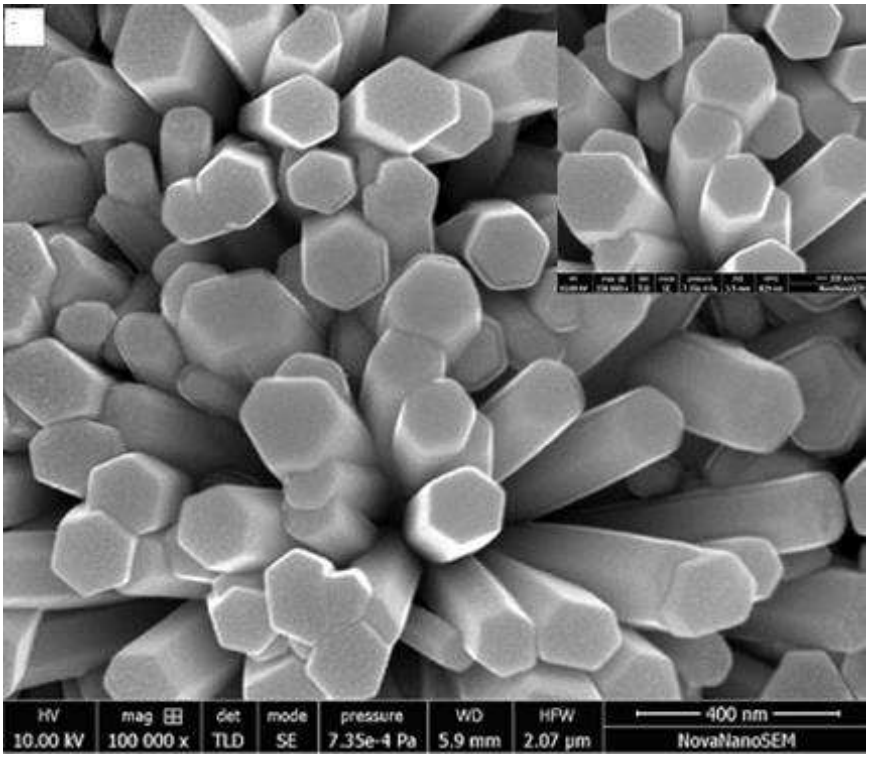

Fig.4.2: ZnO nanorods high resolution SEM (HRSEM) image as grown on FTO substrate at 400 nm scale with magnified version at 100 nm scale shown at the inset.

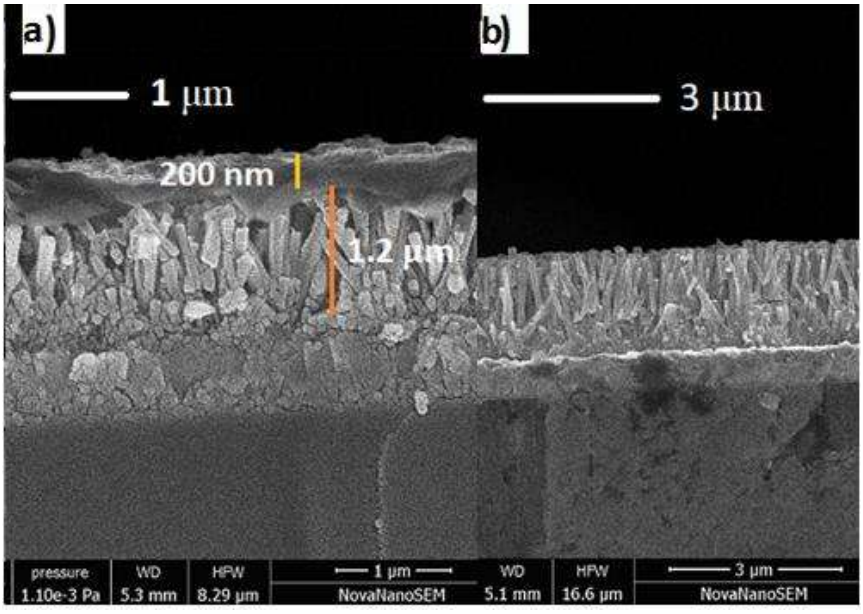

Fig.4.3: (a) Cross sectional FE-SEM image of ZnO NRs/PTB7 bilayer layer; (b) Cross-sectional image of the ZnO NRs layer only.

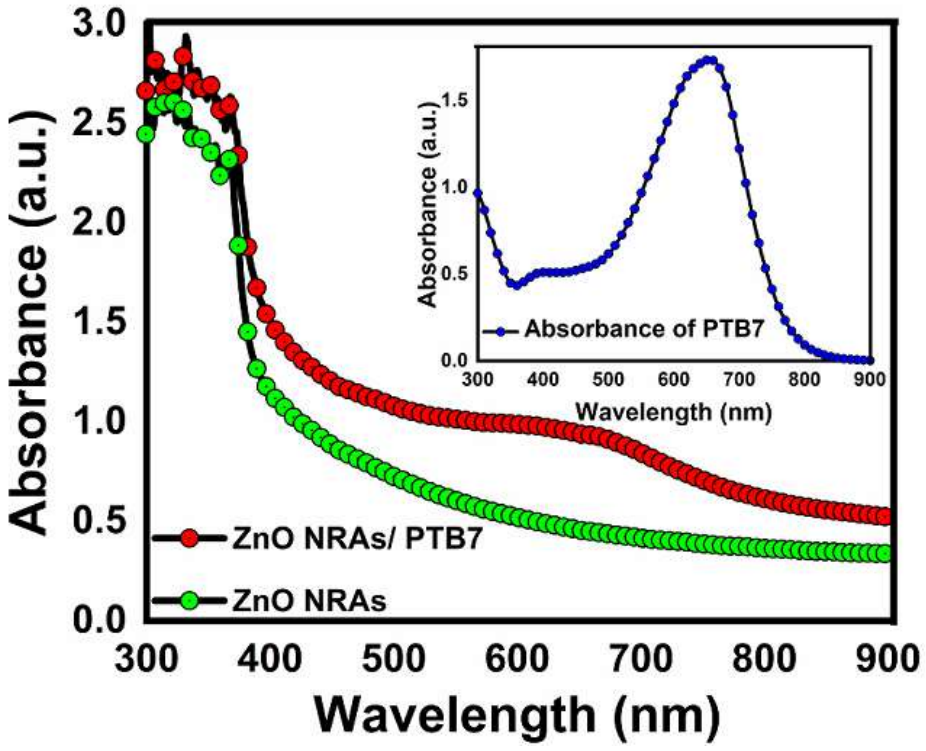

Fig.4.4: The absorption profile of the ZnO NRs layer and ZnO NRs/PTB7 bilayer. Inset sows the separate absorption plot of the PTB7 polymer.

The average thicknesses of n-ZnO NRs and p- PTB7 layers are estimated as ~1200 nm and ~ 200 nm, respectivelyFig.4.4 depicts the absorbance spectra of the ZnO NRs, ZnO NRs/PTB7 and PTB7 (at the inset) obtained from the UV-Vis measurements.The absorption profile of the resultant ZnO NRs/PTB7 bilayer shows a wide absorption range from UV to Visible. The schematic structure and band alignment diagrams of the proposed photodetector are shown in Fig.4.5 (a) and (b). The well aligned energy level diagram confirms the effortless charge transfer in the proposed device structure [92].

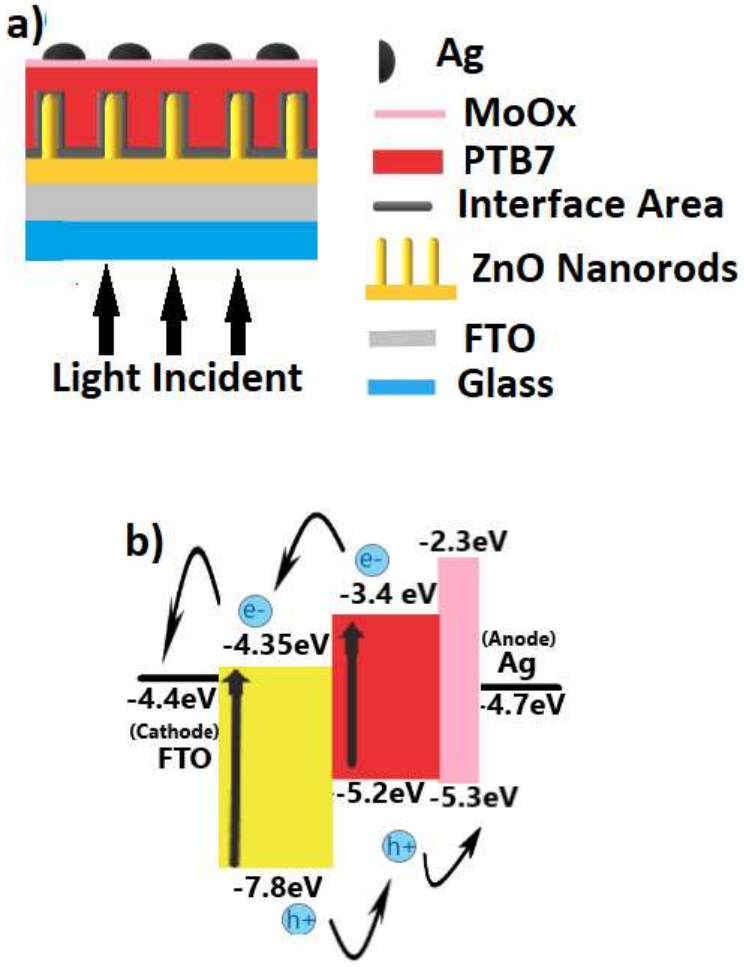

Fig.4.5: (a) The schematic diagram of the fabricated device (b) Depicts the energy level alignment of our proposed device

The charge transfer mechanism in the device is illustrated in Fig.4. 6 .Under equilibrium condition, a small internal electric field exists at the depletion region of the ZnO NRs/PTB7 junction . Under reverse bias, a part of the photogenerated electrons is trapped in the ZnO NRs while the rest is collected by the FTO cathode. The trapped electrons create a Coulomb field which creates a narrow hole injection barrier to assist hole tunneling injection into the device from the cathode [28].

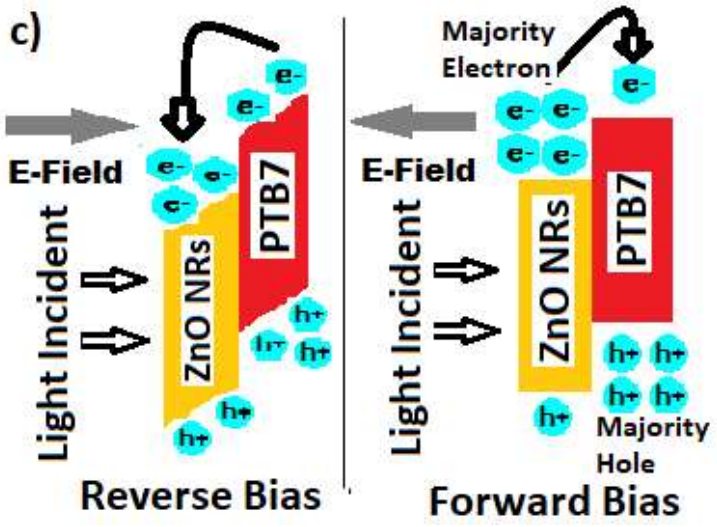

Fig.4.6: Represents energy band diagram with corresponding photo charge carriers transport mechanism at reverse bias and forward bias condition respectively.

These excess injected hole leads to the EQE >100% in our device [59]. On the other hand, photo-generated charge carriers are accumulated under forward bias as shown in Fig.4.6. With the increase in the forward bias or illumination level, these accumulated electrons and holes may jump over the residual barriers to diffuse into the PTB7 and ZnO NRs regions, respectively .

4.3.2 Electrical and Optical Characterization

The electrical characterization of the ZnO NR/PTB7 photodetector were performed by a semiconductor parameter analyzer in an open environment condition (Model name B1500A by Key Sight).The current density (J)-voltage (V) plot (in linear scale) of the device proposed under UV-380 nm light of ~20.07 μWcm^{-2} intensity and under dark are shown in Fig.4.7. Analysis of the J-V characteristics shows notable photocurrent under low reverse bias condition.

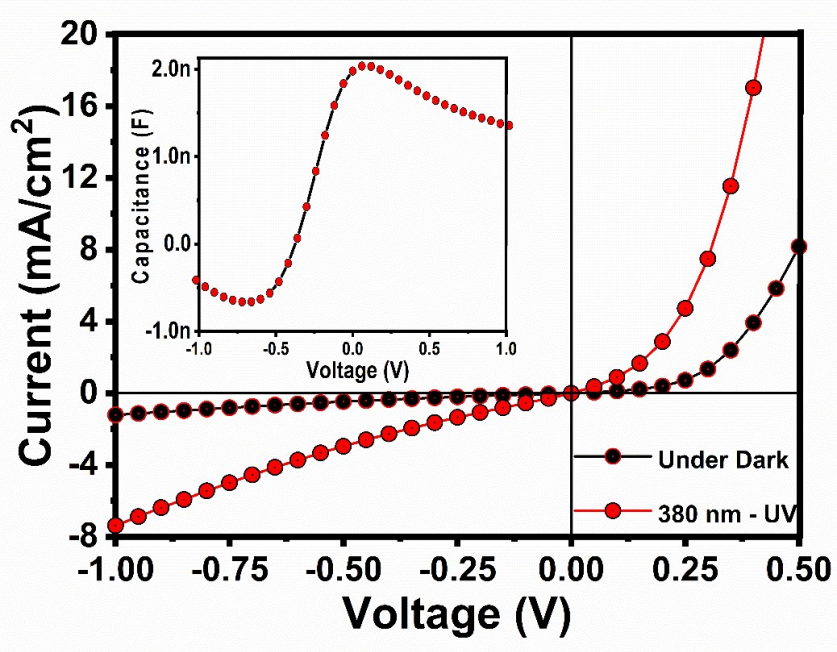

Fig.4.7 Current density -Voltage (J-V) spectra under dark and UV -380 nm illumination of the proposed device in Linear scale. Inset of Fig.4.7 depicts the Capacitance (C)-Voltage (V) plot at 1 MHz frequency

The high current during reverse as well as during forward bias operations as observed from Fig.4.7 support suitable charge injection within the proposed device structure [113]. The capacitance (C)-voltage (V) plot at 1 MHz frequency is also shown in the inset of Fig.4.7. The decreased value of the capacitance with the increased reverse bias voltage is observed due to increase in the depletion region at the ZnO NRs/PTB7 heterojunction interface. The C-V plot thus confirms the formation of heterojunction between ZnO NRs and p-type PTB7 polymer [131]. The corresponding J-V plot in semilogarithmic scale is also shown in the Fig.4.8

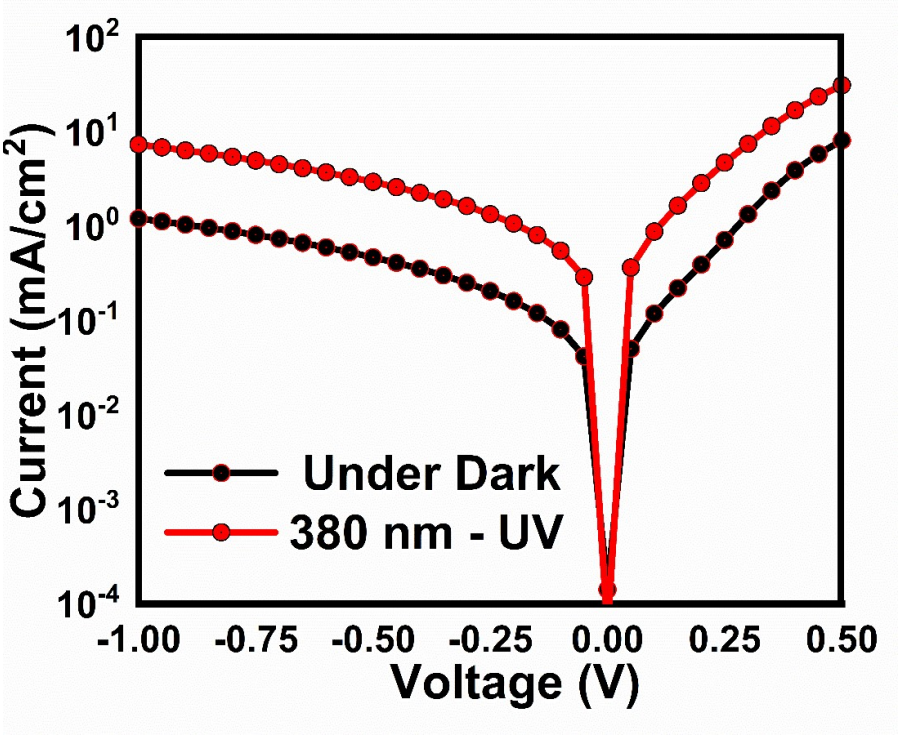

Fig.4.8 : Current density -Voltage (J-V) spectra under dark and UV -380 nm illumination of the proposed device in logarithmic scale.

Furthermore, in order to analyze the repeatability behavior four different devices namely A, B, C and D are fabricated under similar working conditions. The corresponding dark current vs voltage characteristics of the all four devices are compared in Fig.4.9.Interestingly, the close matching of the characteristics of all the devices confirm the repeatability of the performance of our proposed photodetector [132].In addition, no significant performance degradations of the devices were observed within first two weeks after device fabrication.

Monochromator (Serial: Atlas 300-00120, by the Camlin Photonics Limited, Northern Ireland) is used to perform optical characterizations of the device. The responsivity spectra of the photodetector over 300 nm - 900 nm range is shown in Fig.4.10.

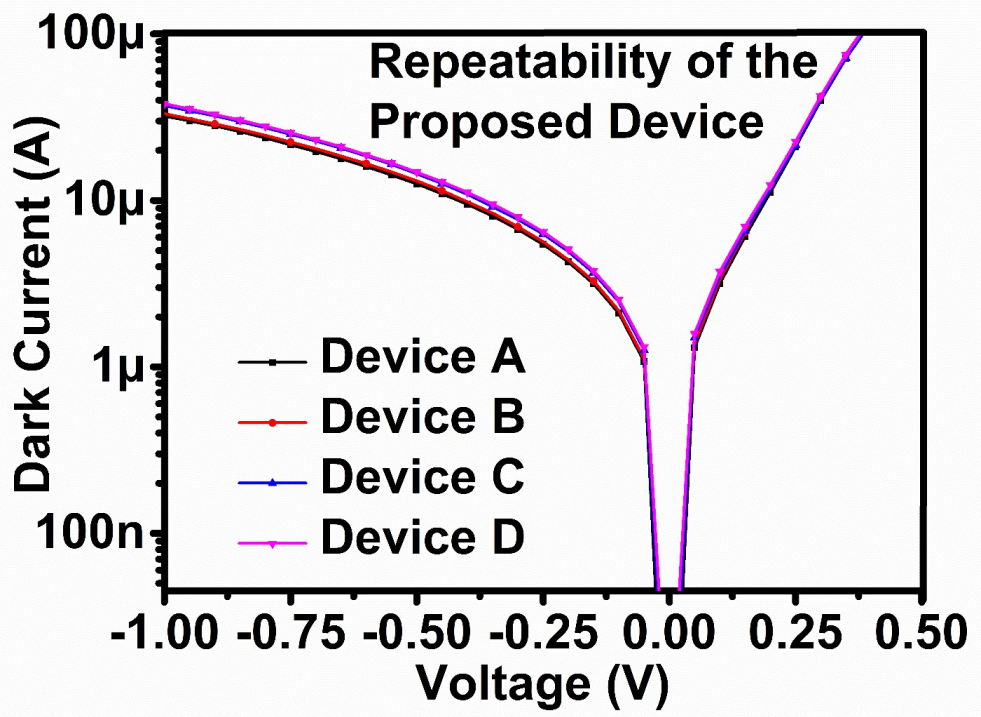

Fig.4.9: Repeatability analysis under similar operating condition dark current - voltage curve of 4 devices.

The responsivity R_λ in A/W was computed using the following equation[89]:

$$R_\lambda(A/W) = \frac{J_{Light} - J_{Dark}}{P_D} \tag{4.1}$$

where J_{Light} denote current Density (A/cm^2) under light, J_{Dark} denote current density (A/cm^2) under dark and P_D denote incident power density (W/cm^2).

Under a low reverse bias voltage of -1V, a high responsivity of ~ 307.18 A/W was measured at wavelength of 380 nm (UV) mainly due to the absorption in the ZnO NRs layer while the responsivity of ~ 33.64 A/W was

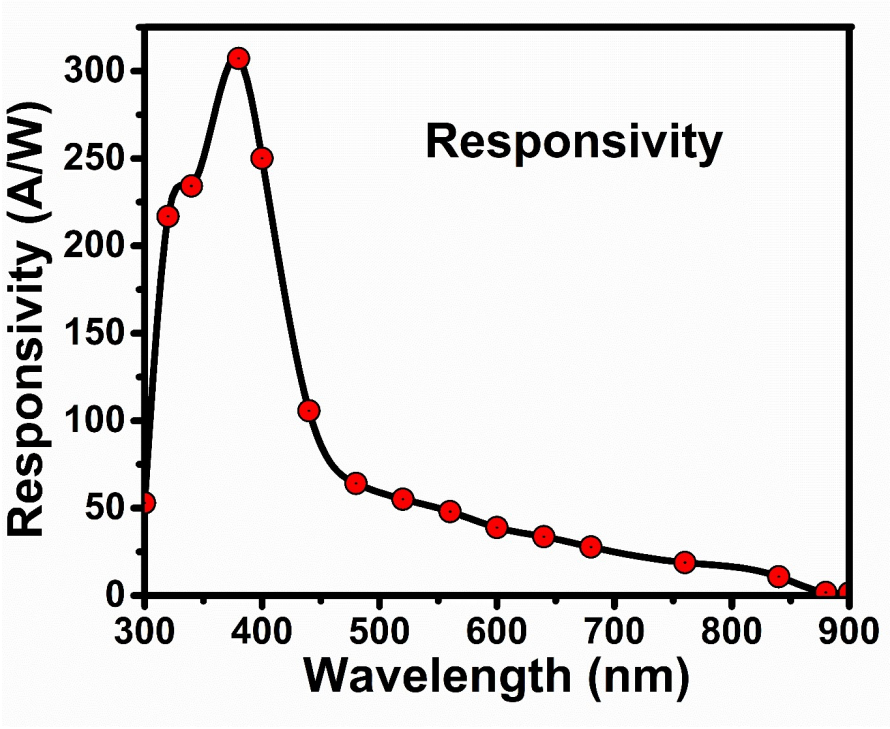

Fig.4.10: .Responsivity plot over spectral range from 300 nm - 900 nm wavelength.

measured at 640 nm (visible) mainly due to absorption of light in p-type PTB7 polymer layer as discussed earlier related to the results shown in Fig. 4.4.Note that PTB7 polymer layer here serves as the active material (for visible region absorption) as well as it serves the purpose of an efficient HTL of the device. On the other hand, the ZnO NRs layer serves as the active material (for absorption in the UV region) as well as an effective ETL of the proposed photodetector. The calculated responsivity of our proposed device is compared with other ZnO NRs/polymer-based heterojunction photodetectors reported in the literature in Table 4.1. Clearly, our proposed device shows much higher responsivity over the other similar reported ZnO NRs/polymer heterojunction devices.

TABLE.4.1 Comparison of the responsivity with different ZnO NRs/ polymer heterojunction-based photodetectors in the literature.

Materials Used (Structure Type)	**Bias (V), T_r/T_f (s)**	**Photo Current to dark current Ratio, P_D (mW/cm^2)**	**Responsivity (A/W)**	**Ref.**
ZnO NRs/PTB7 (Vertical)	-1, 13.8/15	6.1 , 0.020 1.5 , 0.019	307.18 @ 380 nm 33.64 @ 640 nm	This Work
ZnO NRs/P3HT (Vertical)	-2, -/-	278 , 5	4.99 @ 532 nm	[118]
ZnO NRs/Au/P3HT ZnO NRs/P3HT (Vertical)	-2, -/-	- , 3	17.7 @325 nm 10.7 @325 nm	[129]
ZnO NRs/PEDOT:PSS (Vertical)	-1, 0.27 / 0.28	7.14 , 8 1.78 , 2	0.013 @ 380 nm 0.002 @ 550 nm	[122]
ZnO /PEDOT:PSS (Vertical)	-2 ,-/-	16 , -	0.0647 @ 395 nm	[127]
ZnO NRs/PVK (Vertical)	-5, -/-	- , 1.2	0.110 @ 365 nm	[133]
ZnO NRs/PPV-C6 (Vertical)	-, -/-	- , -	0.0293 @ 395 nm	[134]

Furthermore, the detectivity of the device is also plotted vs wavelength over spectral range from 300 nm to 900 nm as shown in the Fig.4.11. The detectivity parameter of our fabricated device is calculated by assuming only shot noise in the device under dark current [30]. The EQE (%) is also shown in the Fig.4.11. The detectivity (D) and EQEs values are computed from the following relations [135]:

$$D(Jones) = \frac{R_\lambda}{\sqrt{2eJ_d}}$$

$$EQE(\%) = 1240\frac{R_\lambda}{\lambda} * 100$$

where, R_λ (A/W) denote the responsivity at wavelength λ and *e* denote the elementary charge.

The measured detectivity (D) at 380 nm is ~1.56x10^{13} Jones and ~1.7x10^{12} Jones at 640 nm under a low -1 V of reverse bias.

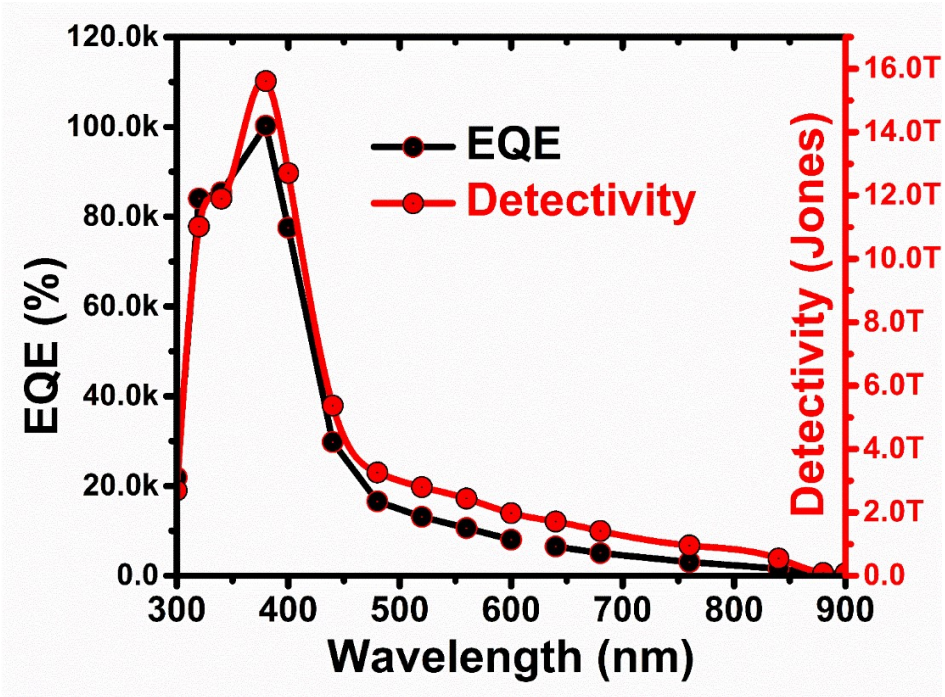

Fig.4.11: .EQE and Detectivity Plot as a function of wavelength over broad spectral range from rom 300 nm - 900 nm wavelength.

The values of the EQE are computed as ~100.23x10^3 % and ~6.51x10^3 % at 380 nm and 640 nm of wavelength respectively. The high EQE of more than 100% in our proposed device is attributed to the enhanced hole injection from the cathode under reverse bias due to photoelectron trapping in ZnO NRs ETL [28] as discussed earlier. The hole injection as well its transportation plays a critical role in deciding the overall performance of the device .In this regard the employed PTB7 basically assist the effective collection of these excess injected holes due to its excellent hole transport property and thus result in a high EQE of the propose device.

In order to get more understanding into the device performance, response speed is also obtained in terms of the rise time and fall (decay) time measurements. Fig.4.12 (a) shows the photoresponse under an on/off modulated light of 380 nm with ~20.07 μWcm^{-2} intensity. The corresponding rise time of ~13.8s and fall time of ~15s were measured from Fig.4.12 (b) from the response of only a single cycle of the incident light. Interestingly, although the device

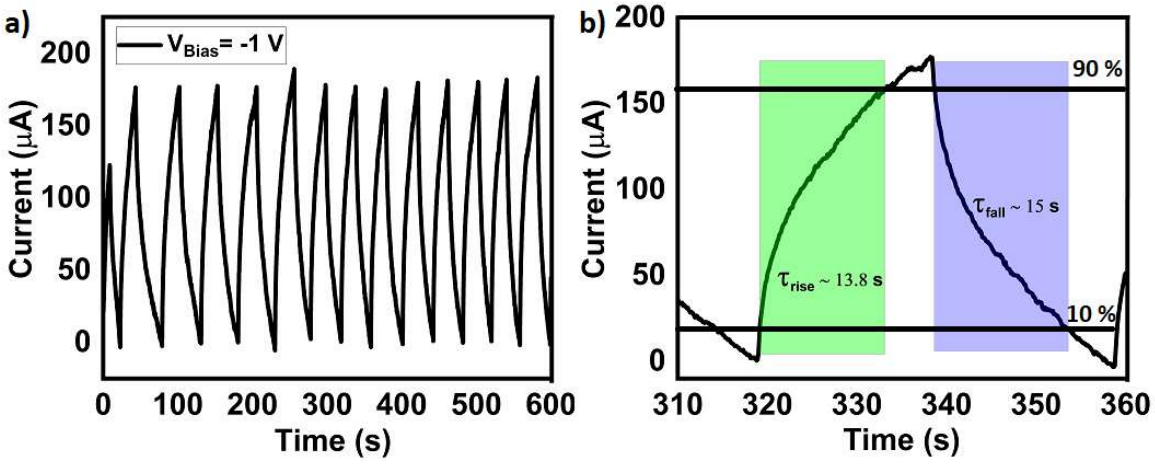

Fig.4.12: (a) Current (I)–Time **(t)** plot under on/off modulated light of 380 nm with ~20.07 μWcm^{-2} intensity (b) Response speed calculations of the device.

parameters such as responsivity, EQE and detectivity is excellent but the measured value of rise time and fall time is bit too large. Herein, it is important to note that, all the fabrication and characterization of our fabricated device were performed under an open environment condition (i.e., without using any controlled Glove Box environment). This may cause some defects in the device which in turn, may deteriorate the response to some extent [114].

4.4 Conclusions

In this chapter, fabrication of a high performance ZnO NRs/ PTB7 heterojunction photodetector using solution method is explored. The PTB7 polymer used in our device has been investigated for detection of light mainly in the visible region while the ZnO NRs layer is used to detect light mainly in the UV region to achieve wideband detection characteristics. The responsivity values are obtained as ~307.18 A/W and ~ 33.64 A/W at 380 nm (UV) light with ~20.07 μWcm^{-2} intensity and 640 nm (visible) light with ~19.12 μWcm^{-2} intensity, respectively, under a low -1 V of operating reverse bias voltage. The values of the detectivity (D) at 380 nm is ~$1.56x10^{13}$ Jones and ~$1.7x10^{12}$ Jones at ~ 640 nm while the computed EQE values are ~$100.23x10^{3}$ % and ~$6.51x10^{3}$ % at 380 nm and 640 nm respectively. The results clearly reveal that PTB7 can be successfully integrated with n-type ZnO NRs for UV-visible wideband photo detection under low external bias and low incident light power.